Fluid conduits formed along burrows of giant bivalves at a cold seep site, southern Taiwan

Jean-Philippe Blouet [a,b] *, Andreas Wetzel [b], Sutieng Ho [c, d] **

[a] *Department of Geosciences, Environment and Society, Université Libre de Bruxelles, Avenue 7 Franklin Roosevelt 50, 1050, Brussels, Belgium;* Email: jeanphilippe.blouet@gmail.com
[b] *Department of Environmental Sciences – Geology, University of Basel, Bernoullistrasse 32, CH-4056, Basel, Switzerland.* Email: andreas.wetzel@unibas.ch
[c] *Ocean Center & Department of Geosciences, National Taiwan University, No. 1, Section 4, Roosevelt Rd, Da'an District, Taipei City, 10617, Taiwan;* Email: sutieng.ho@gmail.com
[d] *Fluid Venting System Research Group, 54000 Nancy, France*

* Corresponding author. Department of Geosciences, Environment and Society, Université Libre de Bruxelles, Avenue 7 Franklin Roosevelt 50, 1050, Brussels, Belgium.
** Corresponding author. Ocean Center & Department of Geosciences, National Taiwan University, No. 1, Section 4, Roosevelt Rd, Da'an District, Taipei City, 10617, Taiwan.

Published: May 11, 2021 in Marine and Petroleum Geology, 131: 105123 (13 p.)
doi: 10.1016/j.marpetgeo.2021.105123

Keywords: Seep carbonate, burrow, methane-derived authigenic carbonate, early diagenesis, lucinid, methane migration, flow channeling, fluid conduit, methane gas chimney, *Anodontia goliath*

Abstract

At a Pliocene methane seep site in Taiwan characterized by numerous tubular carbonate bodies and bivalves, a half meter-long dolomitic concretion containing a lucinid bivalve *Anodontia goliath* reveals the impact of chemosymbiotic bivalves on fluid migration through shallow sediments. The concretion consists of a cortex encasing a central channel filled with sparite and varying amounts of brecciated material derived from the channel walls. The studied bivalve is preserved with the hinge upward. When restored to life position, the central channel is connected to the anterior side of the bivalve. In the lower longer segment, the channel is connected to the posterior sector of the bivalve. The channels are interpreted as the anterior tube for supply of respiration water and the posterior tube for mining sulphide generated in the sulfate-methane transition zone of the sediment. The dolomitic cortex surrounding the central channel is characterized by $\delta^{13}C$ values as low as –29‰ VPDB, indicating that the rate of anaerobic oxidation of methane was enhanced around the conduit. At the base of the central channel, upward soft sediment deformation structures likely resulted from the dragging effect when fluid migrated out of the sediment and entered the channel. Brecciation of the channel walls indicates pulsating seepage during the incipient stages of cementation. The burrow, thus, acted as a highly permeable conduit channeling upstreaming methane-charged fluid for a substantial period of time. Therefore, burrows can be efficient in pre-determining the formation of fluid conduits at seep sites, having potentially a large impact on fluid mixing and diagenetic reaction rates in sediments, and ultimately the amount of methane released. The reported bivalve with its conserved burrow fossilized as seep carbonate concretion provides direct evidence that fluid conduits form along animal burrows.

1. Introduction

Carbonate concretions are common and readily identified in fine-grained marine sediments of various ages (Dietrich, 1999, for a bibliography; Bojanowski et al., 2014; Plet et al., 2016; Lash, 2018). Many of them form during early diagenesis when carbonate oversaturation is favored by microbially mediated anaerobic oxidation of the particulate organic matter within the sediment by seawater compounds, in the order of the decreasing energy yield NO^{3-}, Mn^{4+}, Fe^{3+}, SO_4^{2-}, followed by methanogenesis (e.g., Thullner and Regnier, 2019). This succession of reactions results in a geochemical stratification of the sediment. Within the sulfate-methane transition zone (SMTZ), upward advected or diffused methane produced in the methanogenic zone is oxidized while sulfate is reduced by processes subsumed under the term anaerobic oxidation of methane (AOM; Boetius et al., 2000). Depending on the methane flux, the SMTZ typically develops in a well-defined horizon a few millimeters to several meters below the seafloor (Regnier et al., 2011). In the particular situation at seep sites, methane sourced from deep subsurface reservoirs is added to the methane generated at shallow burial in the sediment by the decay of organic matter, thus enhancing the rate of AOM and pushing the SMTZ up close to the seafloor (Regnier et al., 2011). In such cases, high rates of AOM strongly foster carbonate precipitation by the production of alkalinity and consumption of protons (Blouet et al., 2021a). Such authigenic carbonates are commonly referred to as methane-derived authigenic carbonates (MDAC; Ritger et al., 1987; Hovland et al., 1987; Ho et al., 2012), or seep carbonates (Hecker, 1985; Juniper and Sibuet, 1987). They are often associated with highly specialised chemosymbiotic animals, such as worms and clams (Kiel, 2010; Fischer et al., 2012). In particular, lucinid bivalves harbour sulphide-oxidizing bacteria in their gills that receive sulphide from below via tubes produced by the bivalves while oxygenated water is taken from the seafloor via a mucus-lined tube (Taylor and Glover, 2000).

Tubular carbonate concretions such as chimneys and pipes are ubiquitous features at seep sites; they may reach several meters in length and vary in diameter from a few centimetres to meters (Nyman et al., 2009). They have been reported, for instance, from New Zealand (Campbell et al., 2008; Malie et al., 2017), California (Stakes et al., 1999), Bulgaria (DeBoever et al., 2006), Italy (Viola et al., 2015), Morocco, and Spain (Agirrezabala, 2009), to name a few. Tubes are considered as important components of the 'plumbing systems' of the seep sites because they act as preferential fluid migration pathways (Campbell et al., 2008; Nyman, 2009; Talukder, 2012; Malie et al., 2017; Ho et al., 2018a, b). Through such tubes, rising fluids are quickly expelled to the seafloor and hence, rapidly (by)pass the SMTZ, allowing the release of methane into the ocean. Additionally, fluid channeling triggers the set-up of convection cells in the shallow seafloor sediment, favouring fluid mixing and cementation around the tube (O'Hara et al., 1995; Henry et al., 1996; Santos et al., 2012; Aloisi et al., 2004). The opening of the tubes is commonly interpreted to result from the rising buoyant fluid through a self-generated preferential migration pathway (Martens and Val Klump, 1980; Mazzini et al., 2008; De Boever et al., 2009). More specifically, Aiello (2005) described tubes oriented parallel to pre-existing fractures in the host sediment. Alternatively, Y-shaped tubes belonging to *Thalassinoides/Spongelio-morpha* burrows can act as fluid migration pathway (e.g., Wetzel, 2013; Wiese et al., 2015; Blouet et al. 2017, 2020, 2021b).

In most instances, however, the processes leading to the formation of carbonate-cemented tubes are not investigated in detail or difficult to assess because direct evidence is lacking as they form in the subsurface. The present study addresses the – to our knowledge – so far first case of a lucinid bivalve preserved *in situ* within a vertical dolomitic tubular concretion at a seep-carbonate site. The concretion consists of a central channel surrounded by a cortex having the bivalve enclosed towards one tip. This particular conduit appears to originate from a burrow that was also used as pathway of hydrocarbon-charged fluids. This finding illustrates the important role of burrows as heterogeneities for fluid circulation in near-surface sediments. It is the purpose of the present study to describe this burrow-related methane-seep structure, to elucidate its development, and to decipher its cementation by methane-derived authigenic carbonate.

2. Geological setting

The studied concretion was collected in the area adjacent to the village of Chiahsien (Taiwan), in the lower Pliocene Yenshuikeng Shale Formation. It consists of massive silty mudstone strata with locally intercalated thin sandstone beds deposited in a sublittoral environment of the Neogene Taiwanese foreland basin (Yeh and Chang, 1991) (Fig. 1).

During the ongoing orogeny affecting Taiwan, the Eurasian continent collides with the Luzon volcanic arc, which belongs to the Philippine Sea Plate, moving northwestward and obliquely relative to the Eurasian passive margin at a speed of 8 cm yr^{-1} (Lallemand and Liu, 1998; Byrne and Liu, 2002). Therefore, the geology of Taiwan can be considered as a partly exhumed accretionary wedge (Huang et al., 1997; Liu et al., 2004). Structurally, the Chiahsien outcrop belongs to the Western Foothills of the Taiwanese orogen. They comprise Miocene-Pleistocene marine sediments deposited on the Eurasian margin, which were later incorporated into the accretionary wedge when a series of west-verging thrusts developed during the southward propagation of the arc-continent collision zone. During orogeny, the Western Foothills experienced burial depth typical of the oil window (Sakaguchi et al., 2007).

The seep carbonates in the Chiahsien area have been mapped in detail by Chien et al. (2013). These authors distinguish three types of concretions with respect to their morphology:

(1) 'Massive Brecciated Blocks' representing mound-shaped carbonate bodies having a few meters diameter.
(2) 'Giant Chimneys' being cylindrical or fusiform, several meters in diameter and up to 30 m in height and oriented perpendicular to bedding. An alignment of 'Giant Chimneys' is interpreted by Chien et al. (2013) as formed above a fault used as gas migration pathway.
(3) 'Slender Pipe Networks' consisting of tubular concretions that are preferably oriented perpendicular to bedding, but some branch and extend horizontally. They are commonly between 5 and 15 cm in diameter, but their vertical extent is unknown because they are truncated in the outcrop. They occur isolated and in association with 'Massive Brecciated Blocks' and 'Giant Chimneys'.

The mineralogy of the concretions analyzed by Chien et al. (2013) is dominated by dolomite exhibiting isotope values between endmembers given by $-48‰ < \delta^{13}C < +6‰$ and $-8‰ < \delta^{18}O < +4‰$. The most negative δ13C values are typical of carbonate precipitated from dissolved bicarbonate generated by the anaerobic oxidation of biogenic methane (Hathaway and Degens, 1969; Milkov and Etiope, 2018). Less negative $\delta^{13}C$ values are interpreted to result from a variable mixing of bicarbonate generated by AOM with heavier sources, such as seawater and sedimentary organic matter (Peckmann and Thiel, 2004; Bojanowski, 2012). Positive $\delta^{13}C$ values are attributed to dissolved bicarbonate produced just below the SMTZ by methanogenesis of sedimentary organic matter (Raiswell and Fischer, 2000; Meister et al., 2019). The low $\delta^{18}O$ values are interpreted to represent alteration by meteoric water (Chien et al., 2013).

The tubular concretion addressed in this study ('Slender Pipe' of Chien et al., 2013) has been found in a ~1 m^3-sized mudstone block fallen into a gully downslope from a sector occupied by an isolated

‘Giant Chimney’ that is particularly rich in large globular lucinid bivalves up to 15 cm in size (Fig. 2A; Chien et al., 2013). Originally the bivalves were classified as *Loripes goliath* (Yokoyama, 1928), but later transferred to the genus *Anodontia* (Nomura, 1933; Taylor and Glover, 2009) (Fig. 2B, C, D).

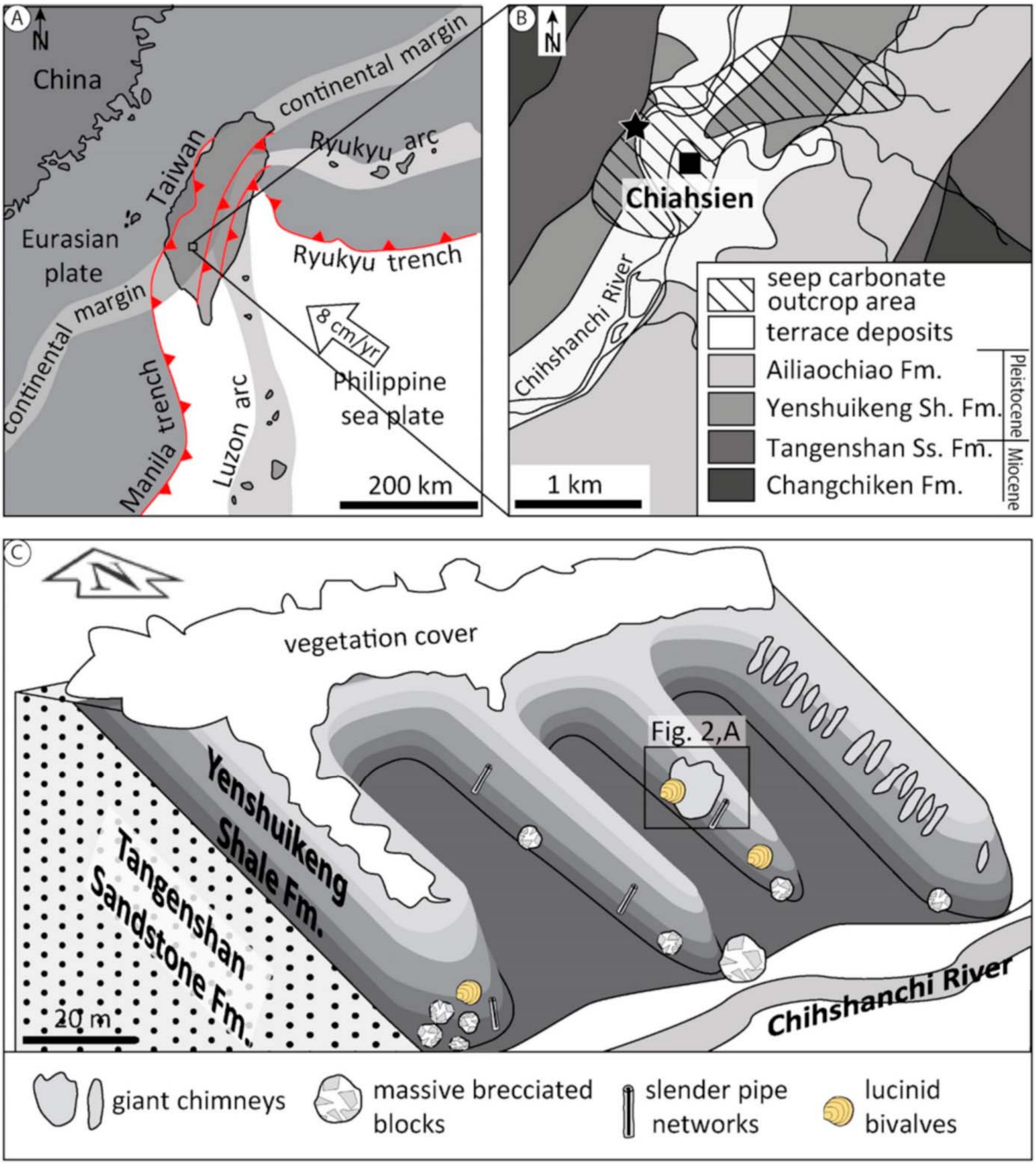

Fig. 1. Geological setting of the outcrop where the studied tubular concretion has been collected. (A) Tectonic scheme of the Taiwan and surrounding areas (modified from Shyu et al., 2005). (B) Geological map of the Chiahsien area where the seep carbonate concretions occur (modified after Sung et al., 2000, and Chien et al., 2013); outcrop marked by star. (C) Schematic representation of the outcrop showing the location of the three morphotypes of concretions and of lucinid fossils (redrawn from Chien et al., 2003).

Fig. 2. Outcrop when studied in 2016. (A) The investigated concretion was collected from a loose block within a gully downslope of an isolated giant chimney; encircled geologist for scale (1.52 m). (B) Tubular concretions within mudstone in the vicinity of the giant chimney. (C) Cluster of *Anondontia goliath* in concretionary limestone of the giant chimney. (D) A tubular concretion with *Anondontia goliath,* close to the base of the giant chimney; this specimen could not be sampled but illustrates *in situ* orientation of the studied concretion.

3. Material and methods

Assemblages of bivalves connected with tubular carbonate concretions were found in the studied site, and the best conserved one has been selected for performing analyses. The studied concretion has been registered under the number of FC0324-113-LIN1 in the Kaohsiung County Jiasian Fossil Museum (Taiwan). The 3D image of the studied concretion can be visualised online (https://fluid-venting-system.org /first-discovered-bivalve-tubular-seep-carbonate).

Eight polished transversal and one longitudinal slabs of the tubular concretion were prepared to accurately observe its internal structures in addition to natural fractures crossing the concretion. In this way the continuity of the structures was proven. The polished sections were examined under natural and 365 nm ultraviolet (UV) light. Three standard thin sections of the central channel, cortex and host rock were investigated by optical microscopy.

For X-ray diffraction (XRD), 6 samples were crushed manually in an agate mortar. The powders were analyzed using a Rigaku Ultima IV diffractometer system using Cu-Kα radiation. The diffractometer is equipped with a position sensitive D-TEX detector and was operated at 40 kV and 40 mA; scans were taken in step scan mode from 5◦ to 70°2θ, with a step interval of 0.01°2θ and a goniometry speed of 0.5°2θ per minute. The identification of all minerals was performed using Rigaku's PDXL-2 software and the ICDD Powder Diffraction File 2017 database (The International Centre for Diffraction Data). Mineral quantification was made by Rietveld refinement (Rietveld, 1969) using the code contained in the same software. The Rietveld method consists in minimizing the difference between a diffractogram calculated for a given starting model (instrument and sample) and the experimental diffractogram. Minimization is done by simultaneously adjusting instrumental and sample parameters by a non-linear multivariable least square procedure. Zero shift and sample displacement were the two instrumental parameters refined in addition to the sample parameter scale factors, unit cell parameters, isotropic temperature factors, as well as coherent single scattering domain sizes. Background intensities were fitted by a seventh order polynomial. Weighted residuals of the whole pattern (Rwp) were taken to indicate the degree of fit between the measured and calculated pattern (Toby, 2006). The Rwp values for the present refinements range from 4.72% to 8.53%.

For oxygen and carbon isotope analysis, 20 samples of carbonate were selected from polished blocks and rock chips using a handheld microdrill under an alternation of natural and UV light. Samples were then analyzed using a Kiel III automated carbonate preparation device coupled to a Finnigan MAT 252 isotope-ratio mass spectrometer. Carbonate material was reacted with 100% phosphoric acid for 10 min at 70°C. Instrumental precision was monitore by analysis of NBS 18, NBS 19, and in some instances LSVEC reference material. Precisions are <0.05‰ for carbon and <0.14‰ for oxygen. Isotope results are given relative to the Vienna Peedee Belemnite standard (VPDB). To check for any spatial variability of the isotope signature within the cortex of the concretion, five regularly spaced samples from center to rim were analyzed. Additionally, two samples of distinctive light intraclasts, two samples from inside the bivalve, and two samples of brecciated clasts within the calcite-filled septarian cracks were investigated. Two representative samples of the Yenshuikeng Shale were collected in vicinity of the isolated giant chimney.

4. Results

4.1. Morphology and structure of the concretion

The retrieved part of the concretion is a ~4 cm wide, ~50 cm long cylinder, but both tips broke away (Fig. 3). Vertical sections of the concretions with downward ramifying *Chondrites* provide evidence of its vertical orientation and indicate the polarity. A globular bivalve about 11 cm in diameter identified as *Anodontia goliath* occurs between an upper, short, 10 cm-long segment of the concretion and a lower, ~30 cm-long segment. The concretion progressively enlarges towards the bivalve without encompassing it completely (Fig. 3A and B). Most of the bivalve is preserved as an internal mold coated in places by a <0.5 mm-thick crust of sparite (Fig. 3C, D, E, F). The anteroposterior axis of the bivalve is oriented parallel to the axis of the tubular concretion, with the anterior side of the bivalve upward (Fig. 3A). The two valves are separated by an up to 1 cm-wide gap at the posterior side. The transition from the concretion to the encasing siltstone is gradual; irregular small-scale furrows and ridges, knobs and depressions along the interface give the surface a rough appearance. Where not covered by host rock, the surface of the concretion exhibits locally faint striations that are almost parallel to its long axis (Fig. 3G and H). Within the lower segment, a reverse shear plane dipping ~35° to the axis of the concretion displaces its lowest part for ~5 cm (Fig. 3G).

The concretion is tubular in shape, consisting of a vertical central channel surrounded by a micritic cortex. The central channel crosscuts all other sedimentary structures. Various trace fossils have been recognized within the cortex (Fig. 4). In nearly all cross-section, *Chondrites* occurs representing 2 size classes having 0.5 mm- and 2 mm-wide tubes, both filled with light, fine-grained sediment. In addition, above the bivalve, there are some curved spreite structures that resulted from the lateral displacement of a nearly horizontal curved tube. These spreite structures are only partly preserved and very likely continued outside the concretion (Fig. 4 B). This fragment is too small to be taxonomically classified. In the lower segment, below the bivalve and at the base of the concretion, few subvertical, irregularly curved tubes occur in the horizontal sections of the concretion (Fig. 4C, H). These burrows are 0.5–0.8 cm in diameter and contain an infill similar to the host sediment. They crosscut *Chondrites.* The outer boundary of these tubes may be transitional to the host sediment, or exhibits some faint lamination organized in a concentric to slightly eccentric pattern (Fig. 4C, H).

The diameter and infill of the central channel vary from the base to the top of the concretion, and the axis of the channel below and above the bivalve is shifted for about 4 cm (Fig. 5A and B). At the base of the lower segment, a funnel-like narrowing-upward structure elongates upward into the central channel (Fig. 4G). The funnel infill consists of millimetric, angular, micritic clasts embedded in a fine-grained matrix. Further up, the matrix progressively turns to a sparry brownish calcite cement. Just above the funnel, the central channel has an elliptical cross-section c. 1.5 × 3 cm in size and is filled to 75–80% by millimetric clasts (Fig. 4F). Further up, about 7–8 cm below the bivalve, sand-sized patches of micrite are arranged over a crescent-shaped coating, lining two thirds of the periphery of the channel, and leaving a circular central area only 0.4 cm in diameter filled with pure sparite (Fig. 4E). Above, the channel widens to 3.5 × 2 cm and contains numerous brecciated clasts (Fig. 4 D). About 2 cm underneath the bivalve, the channel shows a cross-section of 1 × 1.5 cm and it is filled by rhombic clast, 0.3 × 0.7 cm in size cemented by sparite (Fig. 4C). At the lower tip of the bivalve, close to the umbos of the bivalve, the channel continues indistinguishable into septarian cracks. The septarian cracks are filled with brownish sparite containing angular micritic clasts in places. Above the bivalve, the channel emanates at the anterior extremity of the two valves. It is, thus, offset by about 4 cm towards the ventral side compared to the position where it enters the shell from below (Fig. 5A). Above the bivalve, the channel is ~1 cm in diameter and filled for about 3 cm with sparite and milli-

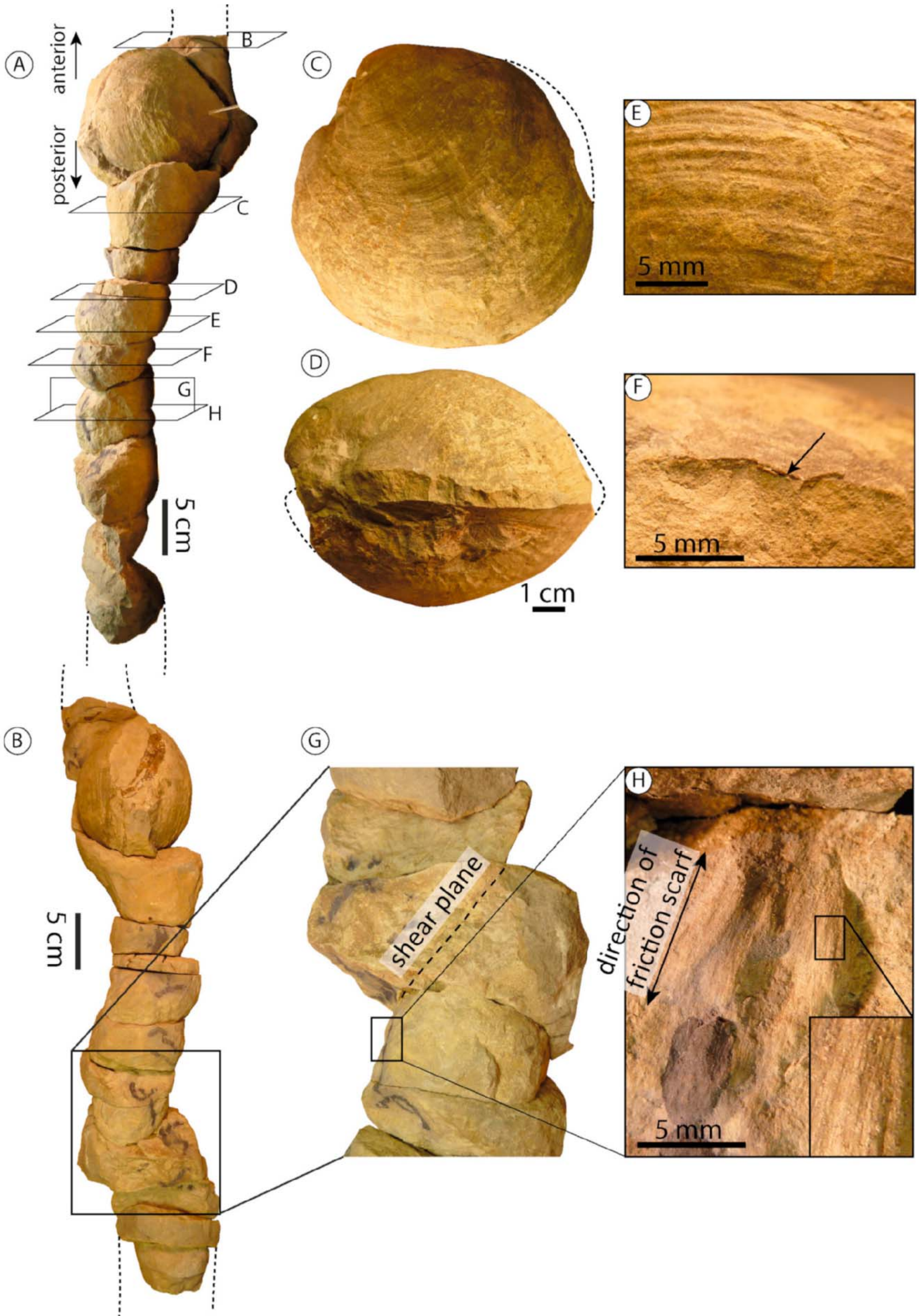

Fig. 3. Concretion housing *Anodontia goliath*. (A) Left side of *A. goliath* within the tubular concretion. (B) Same view as (A), rotated by 90◦, showing *A. goliath* in ventral view; location of cross-sections shown on Fig. 4 indicated. (C) Left side of the *A. goliath*. (D) Anterior view. (E) Low-relief ornamentation of the internal mold of *A. goliath*. (F) Section of the locally molded shell (arrow). (G) Reverse shear plane truncating the concretion. (H) Faint striations indicating the direction of movement along the shear plane.

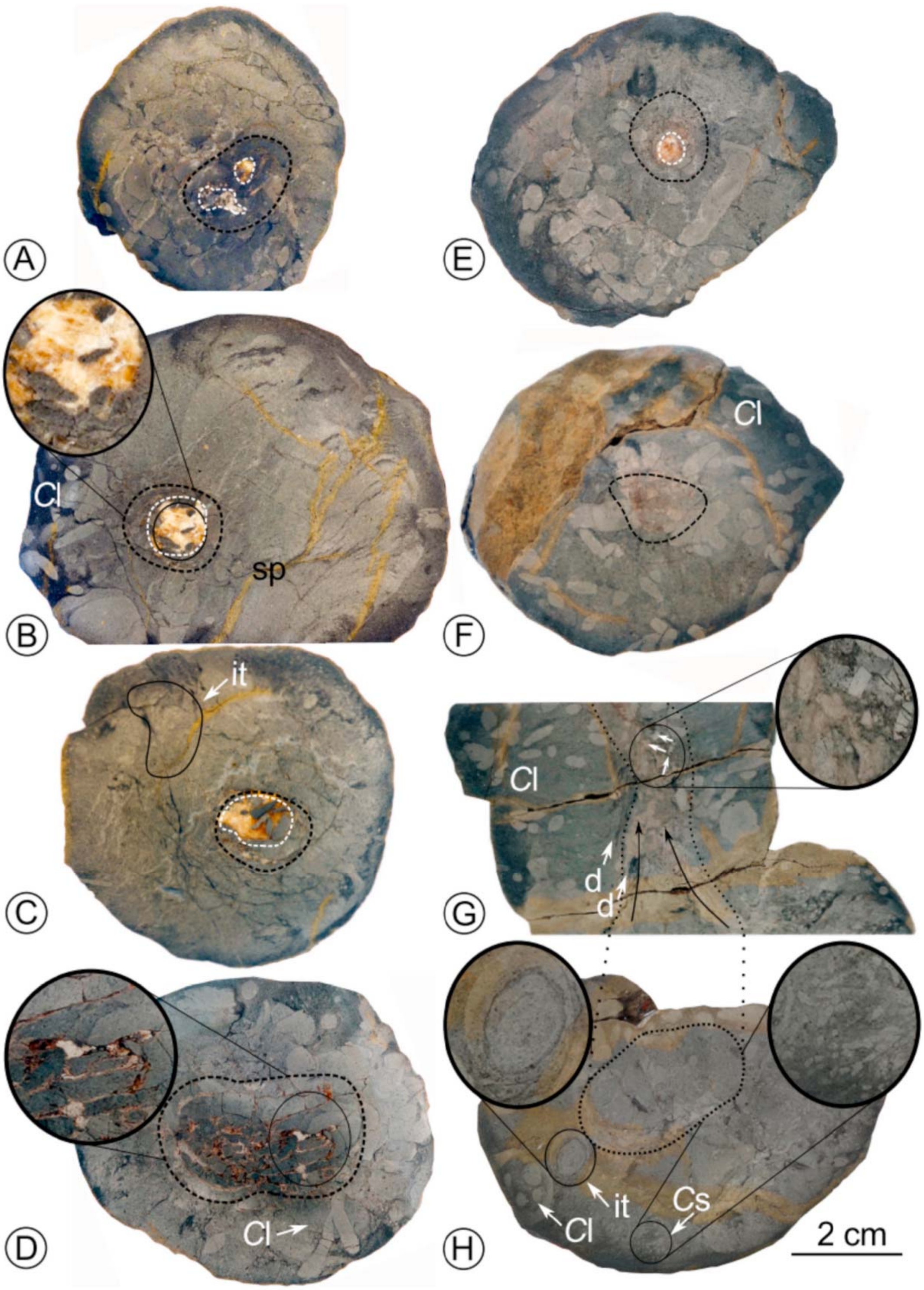

Fig. 4. Sections trough the concretion showing the variability of the central channel from top (A) to base (H) (for position of sections see Fig. 3A); (A), (B) upper concretion segment above the bivalve, (C) to (H) lower concretion segment below the bivalve. Black broken line = outer boundary of the central channel; white broken line = outer boundary of conduit filled with sparite; solid circle = area shown enlarged in inset. (A) Central channel consisting of two small sparite-filled tubes embedded in brecciated material. (B) Wide sparite-filled central channel surrounded by brecciated margin above the bivalve (see inset); *C*l = large *Chondrites*, sp = spreite. (C) as (B) but below the bivalve; it = irregular tube (encircled by solid black line). (D) Central channel filled clasts surrounded by thin sparite rims; *C*l = large *Chondrites*. (E) Sparite-filled central channel surrounded by brecciated wall. (F) Central channel filled with densely packed brecciated clasts; *C*l = large *Chondrites*. (G) Vertical section at the lower tip of the central channel showing an upward-narrowing funnel shape with upward soft-sediment deformation (black arrows) and dragged laminae (d) and further up, brecciated material (white arrows) and shown in inset. (H) Horizontal section of the funnel-shaped structure (encircled by black dotted line); *C*s = small *Chondrites*, it = irregular tube, both shown in inset.

metric, elongate, angular micrite-clasts densely packed at one side of the channel (Fig. 4B). The channel is then partially plugged by an array of millimetric angular micrite-clasts, leaving two circulars opening about 0.3 cm in diameter filled with sparite (Fig. 4A).

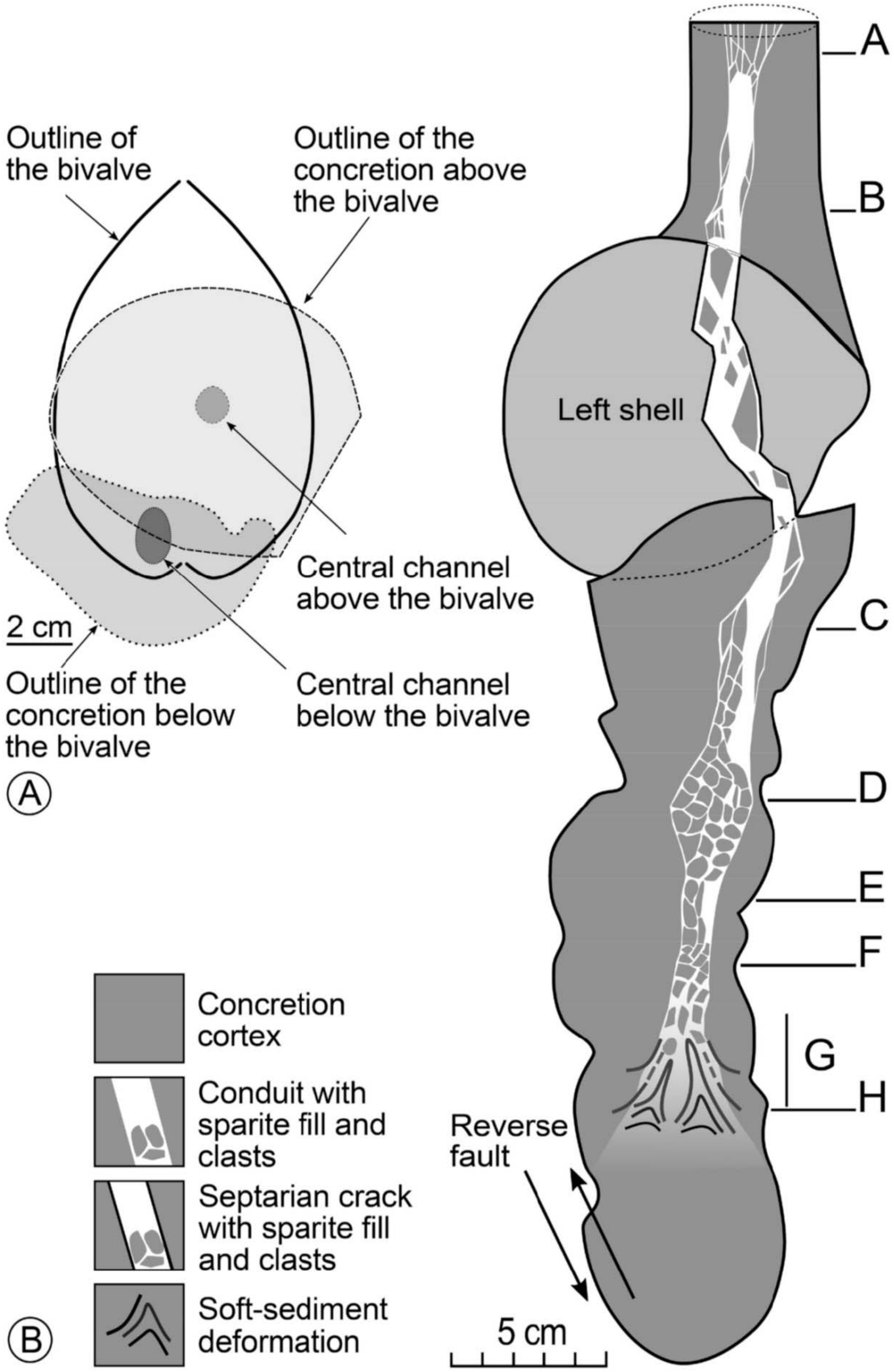

Fig. 5. Schematic diagram showing the geometrical relation between the central channel in the lower long segment of the concretion, the bivalve, and the upper short segment of the concretion.

4.2. Petrography and mineralogy

The Yenshuikeng Shale host sediment consists of well sorted, angular, silt-sized detrital grains (50 µm) exhibiting a packstone texture (Fig. 6A). The cortex of the concretion shows the same composition as the host sediment, cemented by micrite whereas the siliciclastic grains are less densely packed (Fig. 6B). The central tube is filled by weakly cemented siltstone, or brownish sparite, composed of one generation of equigranular 0.5–1.5 cm-sized crystals, which show undulose extinction (Fig. 6C). Brownish sparite also occurs in the septarian cracks inside the *Anodontia* shell. In one thin section, the central tube appears to be lined with mud (Fig. 6C). Some scattered foraminifera, partially pyritized, are present in the host sediment and the cortex of the concretion (Fig. 6D).

XRD analysis reveals a carbonate content of the host sediment of 0–19% (mean 12%), whereas the cortex of the tube is composed of 58–78% (mean 67%) carbonate, partitioned in 82–93% (mean 87%) dolomite and 7–18% (mean 13%) calcite (Table 1). Quartz, albite, and kaolinite are about twice more abundant in the host sediment than in the concretion, whereas the illite content is five times higher. Pyrite and chlorite form accessory components.

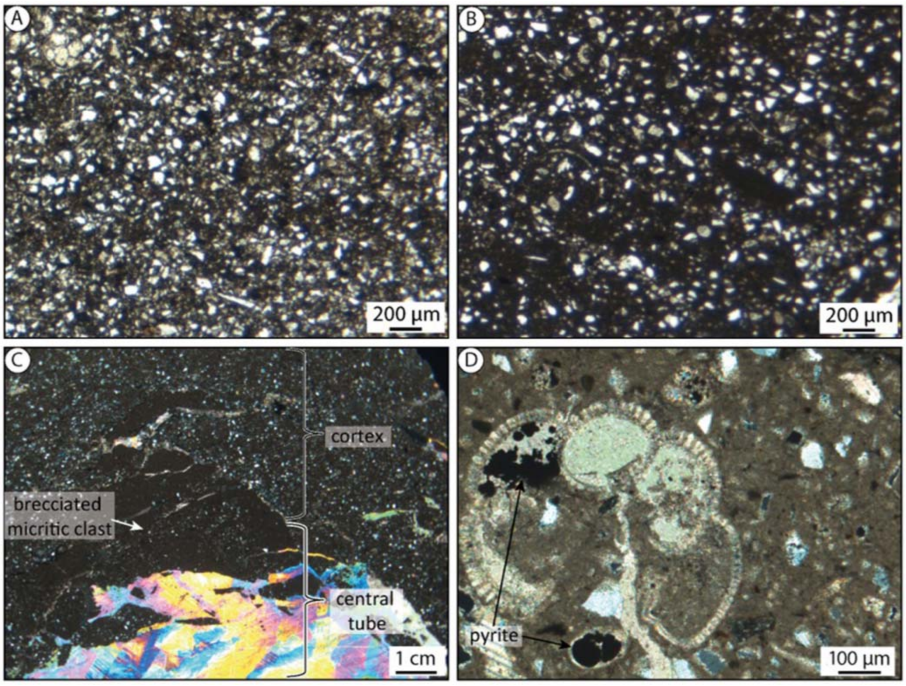

Fig. 6. Photomicrographs illustrating the petrography of the tubular concretion and its host sediment. (A) Host rock (Yenshuikeng Shale). (B) Concretion cortex. (C) Margin of the sparite-filled central tube with some micritic clasts close to the margin. (D) Foraminifera in the cortex, partially filled with pyrite.

Table 1
Mineralogic composition of the tubular concretion, sparitic septarian crack fill, and host rock. The carbon and oxygen isotope data of the corresponding samples is indicated. Rwp: Weighted residuals of the whole pattern; Dol: dolomite; Cal: calcite; Qtz: quartz; Alb: albite; Kln: kaolinite; Ilt: illite; Chl: chlorite; Py: pyrite.

Nature of the sample	Sample ID	Mineralogic composition in weight percent												Isotope data		
		Rwp	Dol	Cal	Qtz	Alb	Kln	Ilt	Chl	Py	Total carbonate	Proportion of carbonates		$\delta^{13}C_{VPDB}$	$\delta^{18}O_{VPDB}$	$\delta^{18}O_{SMOW}$
												Dol	Cal			
Sparite	TW16	4.7	0	100	0	0	0	0	0	0	100	0	100	−13.5	−9.4	20.3
Cortex of the concretion	TW7	6.5	48	10	25	9	3	6	0	0	58	82	18	−25.1	1.7	31.7
	TW8	4.7	55	12	24	7	2	0	0	0	67	82	18	−25.5	1.4	31.4
	TW9	5.2	57	8	17	5	1	12	0	0	64	88	12	−27.3	1.0	31.0
	TW12	5.1	73	5	16	0	3	3	0	0	78	93	7	−28.7	2.5	32.6
	Average	5.4	58	9	20	5	2	5	0	0	67	87	13	−26.7	1.6	31.7
Host sediment	TW1,1	6.8	5	10	41	13	0	21	10	0	16	34	66	−1.4	−9.6	20.1
	TW1,2	7.9	9	10	39	10	10	22	0	0	19	46	54	−1.6	−10.0	19.7
	TW1	6.0	6	6	26	7	12	32	0	11	12	47	53	No analysis		
	TW21	8.5	0	0	49	15	3	31	0	2	0	–	–	No analysis		
	average	7.3	5	7	39	11	6	27	3	3	11.7	42	58	−1.5	−9.8	19.9

4.3. Carbon and oxygen isotope geochemistry

The 2 samples of the host sediment show an average δ^{13}C composition of –1.5‰ and δ^{18}O of –9.8‰. The 6 samples of the cortex of the concretion exhibit an average δ^{13}C isotope signature of –26.9‰ and δ^{18}O of +1.7‰. Narrow sampling from the center to the edge of the cortex does not show considerable variation. Intraclasts, contained in the cortex or the brownish sparite show an average δ^{13}C of –26.6‰ and a δ^{18}O of +2.0‰. The average of the 2 isotope values of the micrite within the bivalve are of δ^{13}C –28,2‰ and δ^{18}O +2.4‰ whereas the bivalve shell has an isotope composition of δ^{13}C –16.5‰ and δ^{18}O –8.8‰. The sparitic septarian fill displays an average isotope signature of δ^{13}C –13,6‰ and δ18O –10.2‰. In summary, the isotope data are arranged in three clusters, comprising (i) host sediment (δ^{13}C – 1.5‰; δ^{18}O –9.8‰) (ii) cortex (δ^{13}C –27‰; δ^{18}O +2‰), and (iii) sparite (δ^{13}C –14‰; δ^{18}O –10‰) (Fig. 7) (Annex 1).

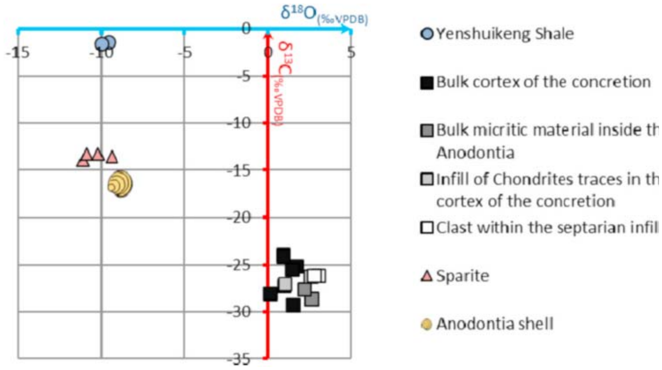

Fig. 7. Carbon and oxygen isotope composition of the tubular concretion, including cortex, intraclasts, bivalve shell, and sparite filling septarian cracks, and the host sediment.

5. Discussion

The association of the tubular concretion and the enclosed lucinid bivalve suggests that concretion formation was related to the burrowing bivalve.

5.1. Carbonate precipitation processes

5.1.1. Depth of precipitation

The cortex of the concretion represents cemented silty host sediment as seen in thin-section analysis. The carbonate of the concretion (67%) is mostly of diagenetic origin as the host sediment contains 12% carbonate. The volume of authigenic carbonate in the concretion (minus-cement porosity = 67%–12%) is about 55% and matches the values of modern silty mud on the seafloor (55–65%; Brückmann, 1989; Wetzel, 1990; Einsele, 2000). Consequently, the concretion became cemented in very shallow burial depth (Lippmann, 1955; Raiswell, 1971; Lash and Blood, 2004), very likely <2–5 m, that compaction did not affect geometry (cross-section) of sediment-filled burrows like *Chondrites* (e.g., Wetzel et al., 1986). Furthermore, the reverse shear plane transecting the concretion most likely resulted from differential compaction during burial because the early lithified concretion resisted compaction relative to the dewatering host sediment (Wetzel, 1992). Striation formed during the shear displacement indicates a movement at an acute angle to the long axis of the tubular concretion and implies a (sub)vertical orientation when it developed.

5.1.2. Diagenetic reactions

The δ^{13}C values of the studied tubular concretion (Fig. 7) broadly match the data obtained for numerous other concretions at Chiahsien seep site (Chien et al., 2013) and other tubular concretions worldwide (Cavagna et al., 2105; Nyman et al., 2010). They are diagnostic of the anaerobic oxidation of methane (AOM). The moderately depleted δ13C values of the studied concretion compared to typical seep carbonates concretions around the world (Peckmann and Thiel, 2004), however, imply a mixing of bicarbonate produced by AOM with heavier one, most likely from seawater (Bojanowski, 2012). Dolomite is the dominant carbonate phase of the studied tubular concretion. This matches the observations made on many other seep-carbonate occurrences including modern and fossil vertical tubular carbonate bodies (e.g., Aloisi et al., 2000; Díaz-del-Río et al., 2003; Takeuchi et al., 2007; Magalhães et al., 2012).

The discrepancy between the proportions of illite in the host sediment and in the cortex of the concretion, compared to detrital minerals such as quartz by a factor of $^{1}/_{5}$ and ½, respectively, imply that illite is mostly of diagenetic origin and formed when the concretion was already fully cemented. This is consistent with the fact that illite is known to forms under oil window conditions (Galán and Ferrell, 2013) and supported by the burial history of the Western Foothills of Taiwan (Sakaguchi et al., 2007).

For oxygen isotopes, the mineral-water equilibrium composition of carbonates ($\delta^{18}O_{Cal}$ for calcite and $\delta^{18}O_{Dol}$ for dolomite) is controlled by the temperature of precipitation (T°K) and by the $\delta^{18}O$ of the precipitating fluid ($\delta^{18}O_{water}$). The fractionation factor between calcite and water ($\Delta_{Cal\text{-}water}$), and between dolomite and water ($\Delta_{Dol\text{-}water}$), can be calculated by using the equation of Friedman and O'Neil (1977) (equation (1)) or of Fritz and Smith (1970) (equation (2)), respectively.

$$\Delta_{Cal–water} = \delta^{18}O_{Cal} – \delta^{18}O_{water} = [(2{,}78*10^{6})/T^{2}] – 2{,}89 \qquad (1)$$

$$\Delta_{Dol–water} = \delta^{18}O_{Do}l – \delta^{18}O_{water} = [(2{,}62*10^{6})/T^{2}] – 2{,}17 \qquad (2)$$

The measured bulk isotopic composition of the cortex $\delta^{18}O_{bulk}$ results of the weighted sum (average of 87%wt dolomite and 13%wt calcite) of the mix of pure dolomite and pure calcite (equation (3)).

$$\delta^{18}O_{bulk} – \delta^{18}O_{water} = (–0{,}13*\delta^{18}O_{Cal} + 0{,}\ 87*\delta^{18}O_{Dol}) – \delta^{18}O_{water} \qquad (3)$$

Assuming that both carbonates precipitated at the same temperature and in isotopic equilibrium with seawater having $\delta^{18}O_{water}$ = 0‰ SMOW then, the temperature of precipitation of the four samples of the concretion cortex for which both mineralogic and isotopic composition have been determined would be 22,8 ± 1,2°C (equation (4))

$$T = \sqrt{\frac{0{,}13*2{,}78*10^{6} + 0{,}87*2{,}62*10^{6}}{0{,}13*2{,}89 + 0{,}87*2{,}17 + \delta^{18}O_{bulk}}} \qquad (4)$$

This temperature is most likely above the temperature on the seafloor and could be explained by seepage of warm or ^{18}O-depleted fluid (Loyd et al., 2012), and/or re-equilibration of oxygen isotope composition during burial. For the late diagenetic calcite in the septarian cracks, characterized by low $\delta^{18}O$ values, a precipitation temperature of 75°C is calculated for a pore fluid having seawater composition. Similarly, the isotopic composition of the calcite material representing the shell mold does not record its original isotopic composition but was precipitated during late diagenesis. The low $\delta^{18}O$ values of the host rock indicate a precipitation temperature of 95°C that implies a dolomitization process of the Yenshuikeng Shale during rather deep burial diagenesis. It is likely that this late episode of dolomitization led to partial re-equilibration of the ^{18}O in the concretion and resulted in an apparent temperature of precipitation above the temperature expected at the seafloor.

5.2. Bivalve burrow and burrowing behavior

All modern specimens of the family Lucinidae, including the genus *Anodontia*, follow a chemosymbiotic mode of live (Taylor and Glover, 2005, 2006). They are burrowers living at the transition of the oxic to the suboxic/anoxic zone in sediment (Fig. 8a), sometimes up to 50 cm deep, and usually vertically oriented with the hinge and umbos uppermost (Fig. 8b) (Taylor and Glover, 2010). The lucinids derive much of their nutrition from symbiosis with sulphide-oxidizing bacteria that is well known through numerous investigations (Taylor and Glover, 2010 and references therein; Gros et al., 2012). The sulphide is collected via one or several tubes produced by the foot penetrating downward while oxygenated respiration water is acquired from the seafloor via an anterior mucus-lined tube that is also produced by the foot because the symbionts have a high oxygen demand (e.g., Taylor and Glover, 2010). In that tube arrangement, *Anodontia* differs from other lucinids, which produce both an inhalant and an exhalant tube to circulate respiration water (e.g., Stanley, 1970). Although most chemosymbiotic bivalves are small, particularly large forms have been recurrently encountered at methane seep sites (Taylor and Glover, 2009, 2010). For instance, modern counterparts to the studied specimen live at active methane seep in the Taiwan Strait, like the giant lucinids *Meganodontia acetabulum* (Bouchet and von Cosel, 2004). Therefore, the exceptionally large size of *Anodontia goliath* implies a habitat being extremely favorable for this bivalve.

Contrary to the common living position of lucinid bivalves having the anterior-posterior axis horizontal and the hinge upward, the studied *Anodontia goliath* specimen is rotated by about 90◦ having the anterior-posterior axis parallel to the axis of the tubular concretion (Fig. 3) (see also Fig. 8b-c). Many lucinid bivalves need to rotate their shells for burrowing ('rocking', Allen, 1958) or for maintenance of the anterior and posterior tubes as the foot needs to be shifted (Allen, 1958). Therefore, it can be speculated that the shell was rotated to respond, for instance, to a depositional event that blocked the connection to the seafloor and hence, respiration water supply (Fig. 8b-c).

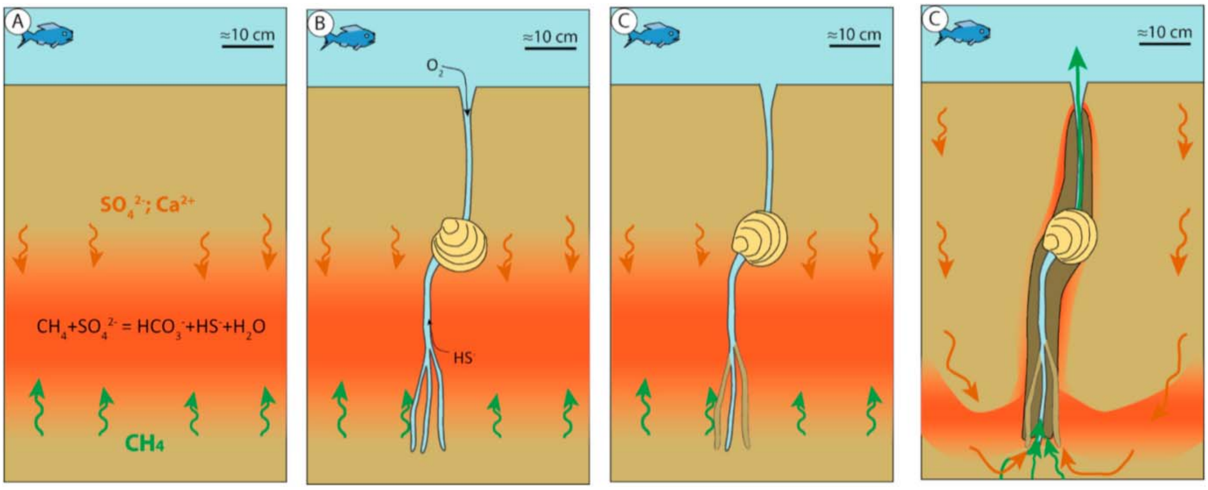

Fig. 8. Steps of cementation of an *Anondontia goliath* burrow. (A) Methane seeps upward and reacts with seawater sulfate a few tens of centimeters below the seafloor, defining the sulfate methane transition zone (SMTZ). The reaction produces sulfide and dissolved bicarbonate. Bicarbonate typically reacts with seawater calcium and magnesium ions to precipitate carbonate, sulfide may precipitate as iron sulfide if reactive iron is available in the sediment, or remains in solution. (B) *Anodontia goliath* settles just above the SMTZ; as for any lucinid, the umbos are upward and tubes are dug downward through the SMTZ to provide sulfide for the symbionts within the bivalve while oxygenated water is inhaled via an anterior, mucus-lined tube. (C) The bivalve tilts its shell by 90◦, possibly for maintenance of the anterior tube in response to a supposed plugging event, and died. (D) After the death, fluid flow channeled into a particular, probably last active, sulfide-mining tube and the mucus-lined anterior tube, forcing the setup of convection cells along the channel and enhancing anaerobic oxidation of methane and cementation along these portions of the tubes.

Alternatively, a decreasing flux of methane and the resulting shortening in sulfide could have forced the bivalve to burrow downward. Both events may have stressed the bivalve and it tried to overcome this situation. In contrast, a tilting of the shell by a vigorous burst of fluid appears rather unlikely due to the friction between the large shell and the host sediment. In addition, the rotated position of the shell is less favorable relative rising fluids. When restored to live position with umbos upward (Fig. 8b), the upper channel within the concretion is situated above the anterior part of the studied *Anodontia* and thus, it is interpreted as the anterior tube produced by the bivalve for supply of respiration water. Similarly, the downward channel within the concretion is connected underneath to the posterior sector of the shell where sulphide can easily reach the gills (Fig. 8b; also Fig. 8c), and matches the typical position of the sulphide mining tubes and hence, is interpreted as such. Very likely, it represented the last open 'sulphide-mining' tube, which acted later as conduit for methane-charged fluids that in turn led to carbonate cementation and brecciation, partially overprinting the original tube (Fig. 8d).

Modern *Anodontia* dig repeatedly 'sulphide-mining' tubes, in particular after a domain has become depleted in dissolved sulphur; after abandonment, a 'sulphide-mining' tube becomes filled and a new one is produced. The nearly vertical tubes displaying laminated margins observed in the vicinity of the channel (Fig. 4H) are interpreted to represent such abandoned tubes. They are similar in size to the central channel and match the observations on modern lucinids that slightly shift these tubes (e.g., Pervesler and Zuschin, 2004). As there is a number of such tubes, they appear to branch downward although branching has not been directly observed. The foot of modern *Anodontia* is about 1/10 to 1/20 of the size of the bivalve that corresponds to the diameter of the tubes (e.g., Lebata et al., 2001; Taylor and Glover, 2009).

The burrow has not been classified taxonomically because its 3D geometry cloud not be exactly evaluated due to later overprint by rising fluids and subsequent brecciation; in particular the arrangement and number of the downward probing tubes as well as the characteristics of the tube providing the connection to the seafloor could not exactly be evaluated. Furthermore, the concretion preserves only part of the whole burrow system. The laminated fill structure of downward tubes (Fig. 4H) would match *Saronichnus* as described by Pervesler and Zuschin (2004). In contrast, underneath the producer, *Saronichnus* should exhibit a peculiar vertical spreite (see Pervesler and Zuschin, 2004: p. 112, Fig. 2). Such a vertical spreite has not been observed in the studied material. The spreite observed in the studied concretion is located above the bivalve and horizontal and can geometrically not be connected to *Anodontia*.

5.3. From burrow to fluid conduit to dolomite tube

As evidenced by the cementation of the sediment surrounding the burrow, rate of anaerobic oxidation of methane and associated carbonate cementation were enhanced along the burrow walls (e.g., Ziljstra, 1995; Stieglitz et al., 2000; Wetzel, 2013). Therefore, the burrow acted as a highly permeable conduit (Fig. 8c). Upstreaming methane-charged fluid moved to a (supposedly) open sulphide-mining shaft, flowed upward, entered the bivalve at the posterior part, traversed the already dead bivalve towards the anterior tube and migrated further up to the seafloor (Fig. 8c). The funnel-like structure at the lower tip of the concretion was likely produced by the dragging effect of fluid migrating out of the sediment and entering the tube (Fig. 8c).

Although several shafts of sulphide mining tubes were possibly available as open pathways for methane-charged fluids up to the surface, it is likely that a phenomenon known as 'flow channelling' focussed the fluid flow along a single path of least resistance (Tsang and Nerethieks, 1998; Eaton, 2006). Very likely, the tube used last for sulphide mining remained open, developed into a channel for methane-charged fluids, and carbonate was precipitated around it whereas non-irrigated shafts became or were already plugged with sediment. Brittle deformation may occur in semi-consolidated or partly cemented material if fluid release is pulsed (e.g., Iadanza et al., 2013) that is commonly observed at seep sites (Leifer et al., 2004; Tryon and Brown, 2004; Saffer and Tobin, 2011). Depending on flow velocity within the channel and stability of its wall, brecciation affected the cross-sectional geometry of the channel as parent feature of the incipient concretion. Upward channel flow probably induced the setup of convection cells in the sediment surrounding the concretion, favouring mixing of seawater and methane-charged fluid and thus, enhancing cementation (O'Hara et al., 1995; Henry et al., 1996; Santos et al., 2012; Aloisi et al., 2000). According to the reaction transport model of Blouet et al. (2021a), the rate of precipitation of an authigenic carbonate crust, in a shelf setting (200 m water depth), and for advection speed of methane-charged fluids commonly encountered at seep sites (5–100 cm yr^{-1}; Regnier et al., 2011) is in the order of 2–14 cm kyr^{-1}. The model of Blouet et al. (2021a), however, does not take into account the effects of convection that rather likely enhances the rate of precipitation. Nevertheless, the time necessary to precipitate a 2 cm-thick carbonate cortex around a conduit definitely exceeded the lifetime of a bivalve. The burrow, thus, remained an active fluid pathway over a significant time period and was still open when the septarian cracks formed in a still plastic concretion (Wetzel, 1992) and when the sparite precipitated during burial diagenesis.

6. Conclusions

A lucinid bivalve *Anodontia goliath* cemented in a tubular carbonate concretion in the Pliocene seep carbonate outcrop of Chiahsien (Taiwan) illustrates the role of burrows as heterogeneities within the seafloor sediment fostering flow channeling at methane seep sites. As any lucinid, *Anodontia goliath* most likely settled close to the sulfate methane transition zone (SMTZ), located centimeters to tens of centimeters below the seafloor. There, it excavated downward posterior tubes exceeding 25 cm in length to mine sulfide generated within the SMTZ. The bivalve also excavated an upward-directed anterior tube for respiration water supply. In normal living position, *Anodontia* is oriented with the umbos upward, but the studied bivalve rotated by 90◦ in posterior direction very likely as it burrowed or maintained the anterior tube just before dying. After the death of the animal, a sulfide mining tube and the anterior tube served as open pathways for ascending fluids and channeled them within a single preferential path-of-least-resistance along that anaerobic oxidation of methane triggered the precipitation of the carbonate cortex. Cementation lasted substantially longer than the lifespan of a bivalve and therefore, the burrow remained a preferential fluid migration pathway for a relatively long period. Consequently, burrows can play an important role as long-lasting open pathway for the release of methane-charged fluids into the ocean at seep sites.

Declaration of competing interest

The authors declare that they have no known competing financial interests or personal relationships that could have appeared to influence the work reported in this paper.

Acknowledgements

The Jiaxian local government and it's community, and in particular the mayor Jianyi Xiao, Liying Huang (黃麗英), Mingchang Yang, Yongfu You, and Junjine Huang, are warmy thanked for their assistance on the field and their hospitality. B. Grobety (Fribourg, Switzerland) is thanked for his help in interpretation of the XRD data. G. Cane (Urbana, Illinois, U.S.A.) is thanked for his special care to provide the carbon and oxygen isotope analyses in really short time. This research did not receive any specific grant from funding agencies in the public, commercial, or not-for-profit sectors. S. HO greatly appreciates the support provided by Prof. Martin Hovland, Prof. Char-Shine Liu, the Ministry of Science and Technology of Taiwan (MOST1052914I002069A1), and the Ocean Center of National Taiwan University.

Annex 1 Carbon and isotope data

Sample ID	Description	$\delta^{13}C_{VPDB}$	$\delta^{18}O_{VPDB}$	$\delta^{18}O_{SMOW}$
TW1,1	host sediment (Yenshuikeng Shale)	−1,4	−9,6	20,1
TW1,2	host sediment (Yenshuikeng Shale)	−1,6	−10,0	19,7
TW2	bulk cortex	−23,9	0,9	30,9
TW3	infill of *Chondrites* in the cortex	−26,2	2,5	32,6
TW4	infill of *Chondrites* in the cortex	−27,1	1,0	31,0
TW5	Sparite	−13,9	−11,1	18,5
TW6	bulk cortex	−24,1	0,9	30,9
TW7	bulk cortex	−25,1	1,6	31,7
TW8	bulk cortex	−25,5	1,4	31,4
TW9	bulk cortex	−27,3	0,9	31,0
TW10	bulk cortex	−28,1	0,1	30,1
TW11	bulk cortex	−29,3	1,5	31,5
TW12	micrite material inside the Anodontia	−28,7	2,5	32,6
TW13	micrite material inside the Anodontia	−27,6	2,2	32,2
TW14	clast within the septarian infill	−26,1	3,0	33,1
TW15	clast within the septarian infill	−26,1	2,7	32,8
TW16	Sparite	−13,5	−9,4	20,3
TW17	Sparite	−13,3	−10,9	18,7
TW18	Sparite	−13,3	−10,2	19,5
TW23	Anodontia shell	−16,5	−8,8	20,9

Appendix Supplementary data

Supplementary data to this article are online at https://doi.org/10.1016/j.marpetgeo.2021.105123.

References

Agirrezabala, L.M., 2009. Mid-Cretaceous hydrothermal vents and authigenic carbonates in a transform margin, Basque-Cantabrian Basin (western Pyrenees): a multidisciplinary study. Sedimentology, 56, 969–996.

Aiello, I.W., 2005. Fossil seep structures of the Monterey Bay region and tectonic/ structural controls on fluid flow in an active transform margin. Palaeogeography, Palaeoclimatology, Palaeoecology, 227, 124–142.

Allen, J.A., 1958. On the basic form and adaptations to habitat in the Lucinacea (Eulamellibranchia). Philosophical Transactions of the Royal Society London, Series B, Biological Science, 241, 421–484.

Aloisi, G., Pierre, C., Rouchy, J.-M., Foucher, J.-P., Woodside, J., 2000. Methane-related authigenic carbonates of eastern Mediterranean Sea mud volcanoes and their possible relation to gas hydrate destabilisation. Earth and Planetary Science Letters, 184, 321–338.

Aloisi, G., Wallmann, K., Haese, R., Saliege, J.-F., 2004. Chemical, biological and hydrological controls on the 14 C content of cold seep carbonate crusts: numerical modeling and implications for convection at cold seeps. Chemical Geology, 213, 359–383.

Blouet, J.-P., Imbert, P., Foubert, A., 2017. Mechanisms of biogenic gas migration revealed by seep carbonate paragenesis, Panoche Hills, California. American Association of Petroleum Geologists Bulletin, 101, 1309–1340.

Blouet, J.-P., Arndt, S., Imbert, P., Regnier, P., 2021a. Are seep carbonates quantitative proxies of CH_4 leakage? Modeling the influence of sulfate reduction and anaerobic oxidation of methane on pH and carbonate precipitation. Chemical Geology, 577: 120254.

Blouet, J.-P., Imbert, P., Foubert, A., Ho, S., Dupont, G., 2021b. From seep carbonates down to petroleum systems: an outcrop study from the southeastern France Basin. American Association of Petroleum Geologists Bulletin, 105, 1033–1064.

Blouet, J.-P., P. Imbert, S. Ho, A. Wetzel and A. Foubert, 2021c (in press). What makes seep carbonates ignore self-sealing and grow vertically? Solid Earth. https://doi.org/ 10.5194/se-2020-187.

Boetius, A., Ravenschlag, K., Schubert, C.J., Rickert, D., Widdel, F., Gieseke, A., Amann, R., Jørgensen, B.B., Witte, U., Pfannkuche, O., 2000. A marine microbial consortium apparently mediating anaerobic oxidation of methane. Nature 407, 623–626.

Bojanowski, M.J., 2012. Geochemical paleogradient in pore waters controlled by AOM recorded in an Oligocene laminated limestone from the Outer Carpathians. Chemical Geology, 292–293, 45–56.

Bojanowski, M.J., Barczuk, A., Wetzel, A., 2014. Deep-burial alteration of early-diagenetic carbonate concretions formed in Palaeozoic deep-marine greywackes and mudstones (Bardo Unit, Sudetes Mountains, Poland). Sedimentology, 61, 1211–1239.

Bouchet, P., von Cosel, R., 2004. The world's largest lucinid is an undescribed species from Taiwan (Mollusca: Bivalvia). Zoological Studies, 43, 704–711.

Brückmann, W., 1989. Porosity modeling and stress evaluation in the Barbados ridge accretionary complex. Geologische Rundschau 78, 197–205.

Byrne, T., Liu, C., 2002. Introduction to the Geology and Geophysics of an Arc-Continent Collision, Taiwan. Geological Society of America, Special Paper, 358, 211 p.

Campbell, K.A., Francis, D.A., Collins, M., Gregory, M.R., Nelson, C.S., Greinert, J., Aharon, P., 2008. Hydrocarbon seep-carbonates of a Miocene forearc (east coast basin), north island, New Zealand. Sedimentary Geology, 204, 83–105.

Chien, C.-W., Huang, C.-Y., Lee, H.-C., Yang, K.-M., 2013. Patterns and sizes of authigenic carbonate formation in the Pliocene foreland in southwestern Taiwan: implications of an ancient methane seep. Terrestrial, Atmospheric and Ocean Sciences, 24, 971–984.

De Boever, E., Huysmans, M., Muchez, P., Dimitrov, L., Swennen, R., 2009. Controlling factors on the morphology and spatial distribution of methane-related tubular concretions – case study of an Early Eocene seep system. Marine and Petroleum Geology, 26, 1580–1591.

De Boever, E., Swennen, R., Dimitrov, L., 2006. Lower Eocene carbonate cemented chimneys (Varna, NE Bulgaria): formation mechanisms and the biological mediation of chimney growth? Sedimentary Geology, 185, 159–173.

Díaz-del-Río, V., Somoza, L., Martínez-Frias, J., Mata, M., Delgado, A., Hernandez-Molina, F., Lunar, R., Martín-Rubí, J., Maestro, A., Fernández-Puga, M., León, R., Llave, E., Medialdea, T., Vázquez, J.T.2003. Vast fields of hydrocarbon-derived carbonate chimneys related to the accretionary wedge/olistostrome of the Gulf of Cadiz. Marine Geology, 195, 177–200.

Dietrich, R., 1999. Rock chips: carbonate concretions, part 1. Rocks and Minerals, 74, 266–269.

Eaton, T.T., 2006. On the importance of geological heterogeneity for flow simulation. Sedimentary Geology, 184, 187–201.

Einsele, G., 2000. Sedimentary Basins: Evolution, Facies, and Sediment Budget. Springer Science & Business Media.

Fischer, D., Sahling, H., N¨othen, K., Bohrmann, G., Zabel, M., Kasten, S., 2012. Interaction between hydrocarbon seepage, chemosynthetic communities, and bottom water redox at cold seeps of the Makran accretionary prism: insights from habitat-specific pore water sampling and modeling. Biogeosciences 9, 2013–2031.

Friedman, I., O'Neil, J.R., 1977. Compilation of Stable Isotope Fractionation Factors of Geochemical Interest. US Geological Survey, Professional Paper, 440-kk, 11p.

Fritz, P., Smith, D., 1970. The isotopic composition of secondary dolomites. Geochimica et Cosmochimica Acta, 34, 1161–1173.

Galán, E., Ferrell, R.E., 2013. Chapter 3 - genesis of clay minerals. In: F. Bergaya, G. Lagaly, (Eds.), Developments in Clay Science 1, Elsevier, Amsterdam, pp. 83–126.

Gros, O., Elisabeth, N.H., Gustave, S.D., Caro, A., Dubilier, N., 2012. Plasticity of symbiont acquisition throughout the life cycle of the shallow-water tropical lucinid *Codakia orbiculata* (Mollusca: Bivalvia). Environmental Microbiology, 14, 1584–1595.

Hathaway, J.C., Degens, E.T., 1969. Methane-derived marine carbonates of Pleistocene age. Science 165, 690–692.

Hecker, B., 1985. Fauna from a cold sulfur-seep in the Gulf of Mexico: comparison with hydrothermal vent communities and evolutionary implications. Bulletin of the Biological Society of Washington, 6, 465–473.

Henry, P., Le Pichon, X., Lallemant, S., Lance, S., Martin, J.B., Foucher, J.P., Fiala- M´edioni, A., Rostek, F., Guilhaumou, N., Pranal, V., 1996. Fluid flow in and around a mud volcano field seaward of the Barbados accretionary wedge: results from Manon cruise. Journal of Geophysical Research, Solid Earth, 101, 20297–20323.

Ho, S., Cartwright, J.A., Imbert, P., 2012. Vertical evolution of fluid venting structures in relation to gas flux, in the Neogene-Quaternary of the Lower Congo Basin, offshore Angola. Marine Geology, 332–334, 40–55.

Ho, S., Hovland, M., Blouet, J.-P., Wetzel, A., Imbert, P., Carruthers, D., 2018a. Formation of linear planform chimneys controlled by preferential hydrocarbon leakage and anisotropic stresses in faulted fine-grained sediments, offshore Angola. Solid Earth, 9, 1437–1468.

Ho, S., Imbert, P., Hovland, M., Wetzel, A., Blouet, J.-P., 2018b. Downslope-shifting pockmarks: interplay between hydrocarbon leakage, sedimentations, currents and slope's topography. International Journal of Earth Sciences, 170, 2907–2929.

Hovland, M., Talbot, M.R., Qvale, H., Olaussen, S., Aasberg, L., 1987. Methane-related carbonate cements in pockmarks of the North Sea. Journal of Sedimentary Petrology, 57, 881–892.

Huang, C.-Y., Wu, W.-Y., Chang, C.-P., Tsao, S., Yuan, P.B., Lin, C.-W., Xia, K.-Y., 1997. Tectonic evolution of accretionary prism in the arc-continent collision terrane of Taiwan. Tectonophysics 281, 31–51.

Iadanza, A., Sampalmieri, G., Cipollari, P., Mola, M., Cosentino, D., 2013. The "brecciated limestones" of maiella, Italy: rheological implications of hydrocarbon-charged fluid migration in the Messinian mediterranean basin. Palaeogeography, Palaeoclimatology, Palaeoecology, 390, 130–147.

Juniper, S.K., Sibuet, M., 1987. Cold seep benthic communities in Japan subduction zones: spatial organization, trophic strategies and evidence for temporal evolution. Marine Ecology Progress Series, 40, 115–126.

Kiel, S., 2010. The Vent and Seep Biota – Aspects from Microbes to Ecosystems. Topics in Geobiology, 33. Springer Science & Business Media, 487 p.

Lallemand, S., Liu, C.-S., 1998. Geodynamic implications of present-day kinematics in the southern Ryukyus. Journal of the Geological Society of China (Taiwan) 41, 551–564.

Lash, G.G., 2018. Significance of stable carbon isotope trends in carbonate concretions formed in association with anaerobic oxidation of methane (AOM), Middle and Upper Devonian shale succession, western New York State, USA. Marine and Petroleum Geology, 91, 470–479.

Lash, G.G., Blood, D., 2004. Geochemical and textural evidence for early (shallow) diagenetic growth of stratigraphically confined carbonate concretions, Upper Devonian Rhinestreet black shale, western New York. Chemical Geology, 206, 407–424.

Lebata, M., Hazel, J., Primavera, J.H., 2001. Gill structure, anatomy and habitat of *Anodontia edentula*: evidence of endosymbiosis. Journal of Shellfish Research, 20, 1273–1278.

Leifer, I., Boles, J., Luyendyk, B., Clark, J., 2004. Transient discharges from marine hydrocarbon seeps: spatial and temporal variability. Environmental Geology, 46, 1038–1052.

Lippmann, F., 1955. Ton, Geoden und Minerale des Barrême von Hoheneggelsen. Geologische Rundschau, 43, 475–503.

Liu, C.-S., Deffontaines, B., Lu, C.-Y., Lallemand, S., 2004. Deformation patterns of an accretionary wedge in the transition zone from subduction to collision offshore southwestern Taiwan. Marine Geophysical Researches, 25, 123–137.

Loyd, S.J., Corsetti, F.A., Eiler, J.M., Tripati, A.K., 2012. Determining the diagenetic conditions of concretion formation: assessing temperatures and pore waters using clumped isotopes. Journal of Sedimentary Research, 82, 1006–1016.

Magalhães, V.H., Pinheiro, L.M., Ivanov, M.K., Kozlova, E., Blinova, V., Kolganova, J., Vasconcelos, C., McKenzie, J.A., Bernasconi, S.M., Kopf, A.J., 2012. Formation processes of methane-derived authigenic carbonates from the Gulf of Cadiz. Sedimentary Geology, 243, 155–168.

Malie, P., Bailleul, J., Chanier, F., Toullec, R., Mahieux, G., Caron, V., Field, B., M¨ahlmann, R.F., Potel, S., 2017. Spatial distribution and tectonic framework of fossil tubular concretions as onshore analogues of cold seep plumbing systems, North Island of New Zealand. BSGF-Earth Sciences Bulletin 188, 25.

Martens, C.S., Val Klump, J., 1980. Biogeochemical cycling in an organic-rich coastal marine basin – I. Methane sediment-water exchange processes. Geochimica et Cosmochimica Acta, 44, 471–490.

Mazzini, A., Ivanov, M.K., Nermoen, A., Bahr, A., Bohrmann, G., Svensen, H., Planke, S., 2008. Complex plumbing systems in the near subsurface: geometries of authigenic carbonates from Dolgovskoy Mound (Black Sea) constrained by analogue experiments. Marine and Petroleum Geology, 25, 457–472.

Meister, P., Liu, B., Khalili, A., Böttcher, M.E., Jørgensen, B.B., 2019. Factors controlling the carbon isotope composition of dissolved inorganic carbon and methane in marine porewater: an evaluation by reaction-transport modelling. Journal of Marine Systems, 200, 103227.

Milkov, A.V., Etiope, G., 2018. Revised genetic diagrams for natural gases based on a global dataset of >20,000 samples. Organic Geochemistry, 125, 109–120.

Nomura, S., 1933. Catalogue of the Tertiary and Quaternary Mollusca from the Island of Taiwan (Formosa) in the Institute of Geology and Palaeontology, Tôhoku Imperial University. Part 1. Pelecypoda. Scientific Reports of the Tôhoku Imperial University, Sendai, Japan, Second Series, 16, 1–108.

Nyman, S.L., 2009. Tubular Carbonate Concretions from North Island, New Zealand: Evidence for Hydrocarbon Migration and the Subsurface Plumbing System of Cold Seeps. PhD Thesis, Univerisity of Waikato (New Zealand).

Nyman, S.L., Nelson, C.S., Campbell, K.A., 2010. Miocene tubular concretions in East Coast Basin, New Zealand: analogue for the subsurface plumbing of cold seeps. Marine Geology, 272, 319–336.

O'Hara, S.C.M., Dando, P.R., Schuster, U., Bennis, A., Boyle, J.D., Chui, F.T.W., Hatherell, T.V.J., Niven, S.J., Taylor, L.J., 1995. Gas seep induced interstitial water circulation: observations and environmental implications. Continental Shelf Research, 15, 931–948.

Peckmann, J., Thiel, V., 2004. Carbon cycling at ancient methane–seeps. Chemical Geology, 205, 443–467.

Pervesler, P., Zuschin, M., 2004. A lucinoid bivalve trace fossil *Saronichnus abeli* igen. et isp. nov. from the Miocene Molasse deposits of Lower Austria, and its environmental significance. Geologica Carpathica, 55, 111–115.

Plet, C., Grice, K., Pagès, A., Ruebsam, W., Coolen, M.J.L., Schwark, L., 2016. Microbially-mediated fossil-bearing carbonate concretions and their significance for palaeoenvironmental reconstructions: a multi-proxy organic and inorganic geochemical appraisal. Chemical Geology, 95–108.

Raiswell, R., 1971. The growth of Cambrian and Liassic concretions. Sedimentology 17, 147–171.

Raiswell, R., Fisher, Q., 2000. Mudrock-hosted carbonate concretions: a review of growth mechanisms and their influence on chemical and isotopic composition. Journal of the Geological Society London, 157, 239–251.

Regnier, P., Dale, A.W., Arndt, S., LaRowe, D., Mogollón, J., Van Cappellen, P., 2011. Quantitative analysis of anaerobic oxidation of methane (AOM) in marine sediments: a modeling perspective. Earth-Science Reviews, 106, 105–130.

Rietveld, H., 1969. A profile refinement method for nuclear and magnetic structures. Journal of Applied Crystallography, 2, 65–71.

Ritger, S., Carson, B., Suess, E., 1987. Methane-derived authigenic carbonates formed by subduction-induced pore-water expulsion along the Oregon/Washington margin. Geological Society of America Bulletin, 98, 147–156.

Saffer, D.M., Tobin, H.J., 2011. Hydrogeology and mechanics of subduction zone forearcs: fluid flow and pore pressure. Annual Review of Earth and Planetary Sciences, 39, 157–186.

Sakaguchi, A., Yanagihara, A., Ujiie, K., Tanaka, H., Kameyama, M., 2007. Thermal maturity of a fold–thrust belt based on vitrinite reflectance analysis in the Western Foothills complex, western Taiwan. Tectonophysics 443, 220–232.

Santos, I.R., Eyre, B.D., Huettel, M., 2012. The driving forces of porewater and groundwater flow in permeable coastal sediments: a review. Estuarine, Coastal and Shelf Science, 98, 1–15.

Shyu, J.B.H., Sieh, K., Chen, Y.G., Liu, C.S., 2005. Neotectonic architecture of Taiwan and its implications for future large earthquakes. Journal of Geophysical Research, 110, B08402.

Stakes, D.S., Orange, D., Paduan, J.B., Salamy, K.A., Maher, N., 1999. Cold-seeps and authigenic carbonate formation in Monterey Bay, California. Marine Geology, 159, 93–109.

Stanley, S.M., 1970. Relation of Shell Form to Life Habits of the Bivalvia (Mollusca). Geological Society of America Memoir, 125, 296 p.

Stieglitz, T., Ridd, P., Müller, P., 2000. Passive irrigation and functional morphology of crustacean burrows in a tropical mangrove swamp. Hydrobiologia 421, 69–76.

Sung, Q., Lin, C., Lin, W., Lin, W., 2000. Explanatory Text of the Geologic Map of Taiwan Scale 1: 50,000; Sheet 51. Central Geological Survey, Ministy of Economic Affairs, Chiahsien (Map).

Takeuchi, R., Matsumoto, R., Ogihara, S., Machiyama, H., 2007. Methane-induced dolomite "chimneys" on the Kuroshima Knoll, Ryukyu Islands, Japan. Journal of Geochemical Exploration, 95, 16–28.

Talukder, A.R., 2012. Review of submarine cold seep plumbing systems: leakage to seepage and venting. Terra. Nova 24, 255–272.

Taylor, J.D., Glover, E.A., 2000. Functional anatomy, chemosymbiosis and evolution of the Lucinidae. In: E.M. Harper, J.D. Taylor, J.A. Crame (Eds.), The Evolutionary Biology of the Bivalvia. Geological Society of London, Special Publications, 177, 207–225.

Taylor, J.D., Glover, E.A., 2005. Cryptic diversity of chemosymbiotic bivalves: a systematic revision of worldwide Anodontia (Mollusca: Bivalvia: Lucinidae). Systermatics and Biodiversity, 3, 281–338.

Taylor, J.D., Glover, E.A., 2006. Lucinidae (Bivalvia)–the most diverse group of chemosymbiotic molluscs. Zoological Journal of the Linnean Society, 148, 421–438. T

Taylor, J.D., Glover, E.A., 2009. A giant lucinid bivalve from the Eocene of Jamaica–systematics, life habits and chemosymbiosis (Mollusca: Bivalvia: Lucinidae). Palaeontology 52, 95–109.

Taylor, J.D., Glover, E.A., 2010. Chemosymbiotic bivalves. In: S.Kiel (Ed.) The Vent and Seep Biota. Topics in Geobiology, 33, 107–135.

Thullner, M., Regnier, P., 2019. Microbial controls on the biogeochemical dynamics in the subsurface. Rev. Mineral. Geochem. 85, 265–302.

Toby, B.H., 2006. R factors in Rietveld analysis: how good is good enough? Powder Diffraction 21, 67–70.

Tryon, M.D., Brown, K.M., 2004. Fluid and chemical cycling at Bush Hill: implications for gas and hydrate rich environments. G-cubed 5.

Tsang, C.-F., Neretnieks, I., 1998. Flow channeling in heterogeneous fractured rocks. Reviews in Geophysics 36, 275–298.

Viola, I., Oppo, D., Franchi, F., Capozzi, R., Dinelli, E., Liverani, B., Taviani, M., 2015. Mineralogy, geochemistry and petrography of methane-derived authigenic carbonates from Enza River, Northern Apennines (Italy). Marine and Petroleum Geology, 66, 566–581.

Wetzel, A., 1990. Interrelationships between porosity and other geotechnical properties of slowly deposited, fine-grained marine surface sediments. Marine Geology, 92, 105–113.

Wetzel, A., 1992. An apparent concretionary paradox. Zentralblatt für Geologie und Paläontologie. Teil 1, Allgemeine, Angewandte, Regionale und Historische Geologie, vol. 1991, pp. 2823–2830.

Wetzel, A., 2013. Formation of methane-related authigenic carbonates within the bioturbated zone — an example from the upwelling area off Vietnam. Palaeogeography, Palaeoclimatology, Palaeoecology, 386, 23–33.

Wetzel, A., Aigner, T., 1986. Stratigraphic completeness: tiered trace fossils provide a measuring stick. Geology 14, 234–237.

Wiese, F., Kiel, S., Pack, A., Walliser, E.O., Agirrezabala, L.M., 2015. The beast burrowed, the fluid followed – Crustacean burrows as methane conduits. Marine and Petroleum Geology, 66, 631–640.

Yeh, M., Chang, Y., 1991. The ichnofacies study of the Ailiaochiao Formation, the Changchihkeng Formation, Chiahsien-Meinung area, Kaohsiung. Petroleum Geology of Taiwan, 26, 151–181.

Yokoyama, M., 1928. Mollusca from the oil-field of the island of Taiwan. Report of the Imperial Geological Survey of Japan, 101, 1–112.

Ziljstra, H., 1995. The Sedimentology of Chalk. Notes in Earth Sciences, 54. Spinger Verlag, Berlin, New York, 197 p.